Optics Letters

Low-power and high-speed 2 × 2 thermo-optic MMI-MZI switch with suspended phase arms and heater-on-slab structure

FEI DUAN, KAI CHEN, DA CHEN, AND YONGLIN YU*

Wuhan National Laboratory for Optoelectronics, Huazhong University of Science and Technology, Wuhan 430074, China
**Corresponding author: yonglinyu@mail.hust.edu.cn*

Received 6 November 2020; revised 4 December 2020; accepted 8 December 2020; posted 11 December 2020 (Doc. ID 413747); published 5 January 2021

We propose a 2 × 2 thermo-optic switch with high switching performance. The switch is based on multimode interferometer (MMI) couplers and a Mach–Zehnder interferometer (MZI) structure, where the phase arms are designed as laterally supported suspended ridge waveguides (LSSRWs) with a metallic heater placed on the slab. It is experimentally demonstrated that this switch has a power consumption of 1.07 mW, a thermal time constant ∼4.7 μs, an extinction ratio ∼30 dB, and an insertion loss ∼0.5 dB. Particularly, the corresponding figure of merit (FOM) has been improved by 1 order magnitude compared with general thermo-optic switches. This 2 × 2 thermo-optic MMI-MZI switch may find potential application for network reconfiguration and on-chip optical information processing.

https://doi.org/10.1364/OL.413747

The 2 × 2 optical switch is one of the indispensable components for protection switching, cross connection, dynamic configuration, and variable optical distribution in next-generation intelligent optical networks and information processing systems [1–4]. To satisfy the increasing channel capacity requirements, there is a growing need for a high-integration optical switch module, including 16 × 16, 32 × 32, and 64 × 64 switch modules. Due to the high refractive index (∼3.5) and compatibility with complementary metal oxide semiconductor (CMOS) manufacturing process, the silicon platform is feasible for large-scale integration and commercial application of photonic integrated circuits, such as the switch module [5–7]. Up to now, optical switches based on the silicon platform can be driven by the thermo-optic effect, electric-optic effect, and microelectromechanical system (MEMS) [8]. Compared with the latter two ways, the thermo-optic effect can realize a large tuning range, a small operation voltage, and especially a tuning-independent optical loss for optical switches [9–11]. Although the 2 × 2 thermo-optic switch has a relatively large response time (microsecond scale), it is suitable for dilated switch modules because of its advantages of low loss and high extinction ratio (ER) [12].

The Mach–Zehnder interferometer (MZI) is a widely used structure for 2 × 2 thermo-optic switch, thanks to its broad bandwidth, high wavelength independence, and temperature independence [8,13]. The 2 × 2 thermo-optic MZI switch predominantly comprises two 3 dB couplers and two arms. Commonly, there are two types of 3 dB couplers including the directional coupler and multimode interferometer (MMI). Although the footprint of the MMI is bigger than that of the directional coupler, the MMI has higher fabrication tolerance, wavelength independence, and polarization independence [14–16]. On the other hand, the phase difference of two arms in MZI are controlled by a phase shifter, which utilizes a metallic heater particularly. While a graphene heater may have a higher response speed [17,18], a metallic heater can ensure a higher reliability for application in air circumstances [19]. The heating power inducing a π (180°) phase shift is defined as the power consumption of thermo-optic switch. In order to decrease the power consumption of the 2 × 2 thermo-optic MZI switch, suspended waveguide structures manufactured by etching cladding beneath and around the arms were proposed, by which the power consumption was reduced to less than 1 mW [20–23]. However, the suspended waveguide structure would lead to a large increase of the response time, resulting in an improved figure of merit (FOM) denoted as the product of power consumption (Q_p) and thermal time constant (τ) as described by Eq. (1) [24,25]. Previously, we have proposed a laterally supported suspended ridge waveguide (LSSRW) for the 2 × 2 thermo-optic MZI switch and realized a relatively smaller FOM than those of general thermo-optic MZI switches based on a suspended waveguide [26,27]. Nevertheless, the fabrication tolerance, ER, response speed, and FOM of the switch should be further improved to meet the practical demand of the high-integration switch modules,

$$\mathrm{FOM} = Q_\mathrm{p} \cdot \tau. \tag{1}$$

In this Letter, we designed and fabricated a 2 × 2 thermo-optic MZI switch based on 3 dB MMI couplers, LSSRWs, and a heater-on-slab structure. For this switch, a taper was adopted to connect the multimode waveguide of the MMI and the single-mode waveguide for reducing the optical loss and imbalance of MMI output ports [14,28]. Moreover, two LSSRWs with metallic heaters patterned on one side of waveguides were implemented as the arms of the MZI for decreasing the power

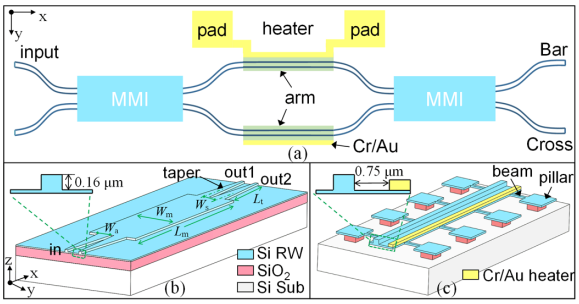

Fig. 1. Schematic of the 2 × 2 thermo-optic MMI-MZI switch: (a) overall structure, (b) MMI, and (c) LSSRW with heater-on-slab structure.

Table 1. Structure Parameters of the MMI

Parameter	W_m	W_a	W_s	L_t	L_m
Dimension (μm)	8.0	2.2	2.67	35.0	78.6

consumption and response time of the switching operation. By silicon microfabrication technology, a 2 × 2 thermo-optic MMI-MZI switch with low power consumption, relatively high response speed, high ER, and low cross talk was demonstrated.

As schematically shown in Fig. 1(a), the 2 × 2 thermo-optic MMI-MZI switch is based on an MZI structure where the MMI is deployed as the coupler. This switch mainly comprises two 3 dB MMI couplers, two symmetric phase arms, and one Cr/Au heater. The overall structure of the MMI [Fig. 1(b)] consists of a multimode waveguide and four taper sections, designed as ridge waveguide (RW) structures on the 0.22-μm-thick top silicon layer of a silicon on insulator (SOI) wafer. As mentioned previously, a taper section is used to connect the multimode waveguide and single-mode waveguide, reducing the optical loss. It is clearly shown in the inset of Fig. 1(b) that the RW has a relatively much thick ridge (0.16 μm) and a thin slab (0.06 μm), focusing the optical energy in the ridge section. The MMI parameters are listed in Table 1. When setting MMI width (W_m) first, MMI length (L_m) and center-to-center separation of two tapers (W_s) can be calculated by Eqs. (2) and (3) [15], where β_1, β_2 are the propagation constants of the first-order mode and second-order mode in the multimode waveguide, and then the length (L_t) and wide side width (W_a) of the taper are attained by simulation optimization using eigenmode expansion method,

$$L_{\mathrm{m}} = \frac{\pi}{2(\beta_1 - \beta_2)}, \tag{2}$$

$$W_{\mathrm{s}} \approx W_{\mathrm{m}}/3. \tag{3}$$

Figure 1(c) depicts the schematic of the LSSRW as two arms of the switch. The LSSRW includes a Cr/Au heater, suspended Si RW, beam-pillar structure, and Si substrate. To improve the device performance, the heater is set on the slab of waveguide, and the thicknesses of Cr and Au layers are 0.01 μm and 0.12 μm, respectively. The length and width of the heater are 100 μm and 0.5 μm, respectively. The spacing between the heater and ridge is designed as 0.75 μm for balancing the optical loss and thermal stability of the waveguide. In order to obtain a single-mode waveguide, the width of the ridge and slab are 0.5 μm and 2.1 μm, respectively. The dimension parameters of the beam-pillar structure, supporting the suspended RW,

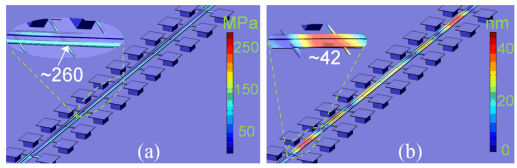

Fig. 2. Simulated distributions of (a) stress and (b) deformation of LSSRW under a temperature rise of 100°C.

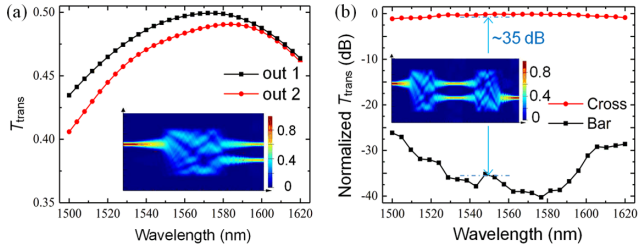

Fig. 3. Simulated transmission (T_{trans}) of the output ports (a) MMI and (b) 2 × 2 thermo-optic MMI-MZI switch without heating on LSSRW. Insets show the optical power distribution at a wavelength of 1550 nm.

have the same values as the devices fabricated before [27]. With the numerical model built previously [29], the simulated distributions of stress and deformation for LSSRWs are obtained by the finite element method and plotted in Fig. 2. Under a temperature rise of 100°C, the maximum stress, occurring in the Au heater layer, is about 260 MPa, which is smaller than the allowable stress of the Au thin film [30]. Meanwhile the maximum deformation (~42 nm), approaching two ends of the LSSRW, is just ~0.4% of the distance between adjacent beam-pillar structures. These results indicate that the 2 × 2 thermo-optic MMI-MZI switch with the LSSRW has a high thermal stability when operation temperature increases 100°C.

To ensure a high ER and small cross talk for the 2 × 2 thermo-optic MMI-MZI switch, it is highly important to balance the output powers of the two ports [out 1 and out 2 shown in Fig. 1(b)] in the 3 dB MMI coupler. Figure 3(a) presents the simulated transmission of these two output ports by the eigenmode expansion method. The splitting ratio between out 1 and out 2 is 1.0–1.06 approximately, indicating that the MMI coupler has a precise 3 db splitting. With these MMI couplers, the corresponding transmission of the two ports (Bar and Cross) in 2 × 2 thermo-optic MMI-MZI switch is illustrated in Fig. 3(b). When not heating one LSSRW in the switch, the Cross port is at on-state while Bar port is off. In the wavelength range of 1510 to 1600 nm, the cross talk between the Cross and Bar is smaller than −30 dB, and especially it is ~ − 35 dB at a wavelength of 1550 nm, presenting a high switching performance.

The fabrication process for the 2 × 2 thermo-optic MMI-MZI switch is shown in Fig. 4. While the first procedure is identical to the previous switch [26], MMI and phase arms are defined on the top silicon layer of SOI by electron beam lithography and inductively coupled plasma etching. Then, the Cr/Au heater layer is deposited on the slab of the phase arms after defining the heater domain by electron beam lithography. Finally, the air trench structure is formed by wet-etching SiO_2 layer with 40%-mass-fraction hydrofluoric acid (~100 s). It is validated in the fabrication that the hydrofluoric acid would nearly not react with Cr/Au. Compared with the fabrication

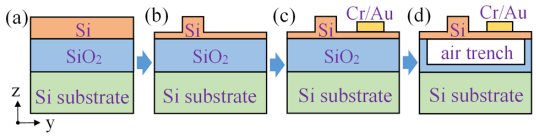

Fig. 4. Schematic of the microfabrication process of the switch: (a) SOI wafer, (b) definition of ridge waveguide, (c) deposition of the Cr/Au heater on the slab, and (d) formation of the air trench beneath the phase arms.

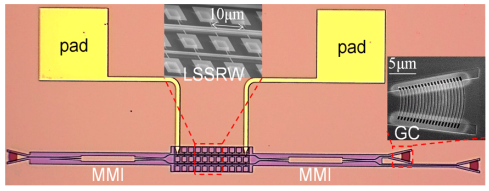

Fig. 5. Microscope image of the overall structure and SEM images of the LSSRWs and grating coupler for the 2 × 2 thermo-optic MMI-MZI switch.

process adopted previously [26], the process presented here has a lower cost and can ensure a higher accuracy for the narrow heater layer because there is no SiO_2 depositing procedure after etching the waveguides and because a thin photoresist is needed for the metal lift-off process. The yield for the switch (three identical devices) is about 100% as e-beam lithography is used for device structure definition in each process.

Figure 5 shows the top view of the fabricated 2 × 2 thermo-optic MMI-MZI switch. The overall structure was obtained by a microscope, while structures of the grating coupler and LSSRWs were characterized by a scanning electron microscope (SEM). The grating coupler is composed of focusing grating that has a period of 0.62 μm and a length of ∼13.0 μm. Owing to the high refractive index contrast in the grating without a SiO_2 upper cladding layer, the measured optical loss of one grating coupler is about −5.5 dB at a wavelength of 1550 nm. LSSRWs are clearly shown in the middle inset, which has robust beam-pillar structures to sustain the suspended waveguide. Note that, despite the metallic pads and grating coupler, the footprint for overall structure is ∼450 μm × 30 μm, suggesting that this switch is applicable to switch modules.

The switching power consumption (Q_p) of the 2 × 2 thermo-optic MMI-MZI switch can be measured by the transmission of two output ports (Cross and Bar). The measurement was conducted by an optical circuit whose light (1555 nm) was transmitted by a semiconductor laser (santec TSL-510), and then went through a polarization controller and the switch; finally, it was detected by an optical powermeter (YOKOGAWA AQ2200-221). Figure 6 shows the normalized transmission of Cross and Bar ports under different heating powers to one LSSRW in the switch. The normalized transmission is equal to the values of subtracting output powers of Cross and Bar ports by the measured output power of two back-to-back grating couplers. The measured average Q_p is ∼1.07 mW for both the Cross and Bar ports. Moreover, the switch has excellent static-state features with an ER ∼30 dB, an insertion loss (IL) ∼0.5 dB, and cross talk as low as −30 dB. The IL is the absolute value of the normalized transmission when the output port of the switch is at on-state and the measurement error of the optical powermeter is ±0.13 dB, which may cause some uncertainty.

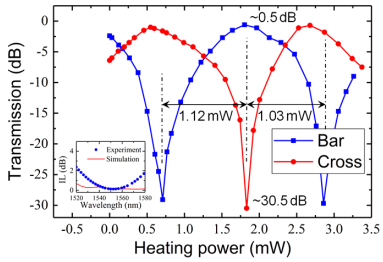

Fig. 6. Measured transmission of the Bar and Cross output ports of the 2 × 2 thermo-optic MMI-MZI switch under different heating powers on one arm. Inset shows the experimental and simulated results of IL.

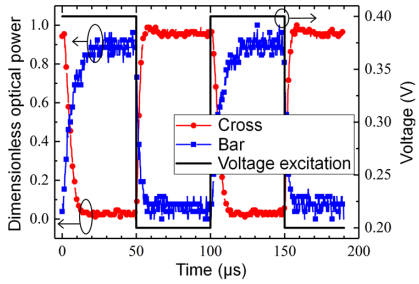

Fig. 7. Measured transient response for the Bar and Cross output ports of the 2 × 2 thermo-optic MMI-MZI switch under 10 kHz square-wave voltage excitation.

It is observed from the measurement and simulation results (inset in Fig. 6) that the IL is smaller than 0.5 dB in a wavelength range of 1540 nm to 1565 nm.

The transient response of the 2 × 2 thermo-optic MMI-MZI switch was measured by a similar circuit described above, but the output light from semiconductor laser was first amplified by an erbium-doped fiber amplifier and finally detected by an optical detector (THORLABS DET01CFC). The voltage excitation added on the heater, and the measured dimensionless optical powers of Bar and Cross ports are plotted in Fig. 7. The voltage excitation has a frequency and a duty cycle of 10 kHz and 50%, respectively, changing between 0.2 V and 0.4 V. The measured 10%–90% rising time (t_{up}) and 90%–10% falling time (t_{down}) are about 10.4 μs and 5.2 μs, respectively. Thus, the thermal time constant ($\tau = t_{up}/2.2$ [25]) is about 4.7 μs. Herein, the transient response process when increasing heating power is defined as the rising process, while the process when decreasing the heating power is the falling process.

The performance comparisons of the switch presented here with the previously fabricated switch [26] and several representative thermo-optic switches are listed in Table 2. Compared with other thermo-optic switches, the thermo-optic switch presented here exhibits a FOM (<10 nW·s) with 1 order magnitude improvement, high ER, small Pi voltage (V_π), and relatively low optical loss. Note that the thermal time constant of the switch presented here is far smaller than that of the previous switch, benefiting from the decrease in heat capacity of the phase arm [29].

In conclusion, we have designed and demonstrated a high switching performance 2 × 2 thermo-optic MMI-MZI switch with a LSSRW and heater-on-slab structure. Deploying the heater on the slab of the LSSRW and maintaining a sufficient

Table 2. Performance Comparison of Typical Thermo-Optic Switches[a]

Work	Structure	Cladding	Heater	L_{WG} (μm)	V_π (V)	Q_p (mW)	τ (μs)	FOM (nW·s)	ER (dB)	IL (dB)
Yu *et al.*[18]	MD	air	graphene	/	~2.6	~4.0	5.8	~23.2	~15	/
Schall *et al.* [17]	MR	Al_2O_3	graphene	~56.6	~7.3	~11.0	1.4	15.4	~10	/
Atabaki *et al.* [9]	MR	air	NiCr	~12.6	~2.8	~12.2	1.3	15.9	~15	/
Dong *et al.* [31]	SMR	SiO_2	Ti	~40	0.5	~1.2	77.3	~92.8	~10	~0.5
Watts *et al.* [24]	MZI	air	$N_{++}Si$	~10	~12	12.7	2.4	30.5	~20	~0.5
Jacques *et al.* [25]	MZI	SiO_2	$N_{++}Si$	~300	~2.2	22.8	2.2	50.2	~30	<0.4
Fang *et al.* [23]	SW-MZI	SiO_2	TiN	120	~0.9	0.49	65.5	32.1	23	0.3
Lu *et al.* [21]	SFW-MZI	SiO_2	TiN	~2750	~0.14	0.05	354.5	17.7	26	3.3
Previous work [26]	LSSRW-MZI	SiO_2	Cr-Cu	100	0.6	1.1	34.5	38.0	11.5	0.5
Present work	LSSRW-MZI	air	Cr/Au	100	0.2	1.07	4.7	5.0	30	~0.5

[a]MD, micro-disk; MR, micro-ring; SMR, suspended micro-ring; SW, suspended waveguide; SFW, suspended folded waveguide; N_{++} Si, n-doped silicon; Cr-Cu, Cr heater layer and Cu pad.

distance between the ridge and heater, the fabricated switch can enable a low power consumption, a relatively fast response, a high ER, and a low optical loss. Moreover, this switch has a 1 order magnitude higher FOM than typical thermo-optic switches. While the optical loss can be further reduced by using a high-accuracy microfabrication process, the 2×2 thermo-optic switch proposed may have a promising application in switch modules for reconfigurable optical network and on-chip optical information processing systems, which need a modest response speed.

Funding. Wuhan International Joint Laboratory on Optoelectronics; National High-tech Research and Development Program (2013AA014503); National Natural Science Foundation of China (61675073).

Acknowledgment. The authors would like to thank Mr. Ming Cheng, Mr. Xiaoping Cao, Ms. Yuedi Ding, and Dr. Cheng Zeng from the Wuhan National Laboratory for Optoelectronics (WNLO) for their help with developing the measurement systems. The authors would also like to thank all the engineers at the Optoelectronic Micro & Nano-Fabrication and Characterizing facility of WNLO for the assistance in device fabrication.

Disclosures. The authors declare no conflicts of interest.

REFERENCES

1. A. M. Al-Hetar, A. B. Mohammad, A. S. M. Supa'At, and Z. A. Shamsan, J. Lightwave Technol. **29**, 171 (2010).
2. D. Dai, D. Liu, and S. Wang, Proc. SPIE **10823**, 108230B (2018).
3. G. Zhang, J. Y. Haw, H. Cai, F. Xu, S. M. Assad, J. F. Fitzsimons, X. Zhou, Y. Zhang, S. Yu, J. Wu, W. Ser, L. C. Kwek, and A. Q. Liu, Nat. Photonics **13**, 839 (2019).
4. J. Wang, F. Sciarrino, A. Laing, and M. G. Thompson, Nat. Photonics **14**, 273 (2020).
5. V. Stojanović, R. J. Ram, M. Popović, S. Lin, S. Moazeni, M. Wade, C. Sun, L. Alloatti, A. Atabaki, F. Pavanello, N. Mehta, and P. Bhargava, Opt. Express **26**, 13106 (2018).
6. Z. Zhang, M. Yako, K. Ju, N. Kawai, P. Chaisakul, T. Tsuchizawa, M. Hikita, K. Yamada, Y. Ishikawa, and K. Wada, Sci. Technol. Adv. Mater. **18**, 283 (2017).
7. J. F. Song, Q. Fang, T. Y. Liow, H. Cai, M. B. Yu, G. Q. Lo, and D. Kwong, *Optical Fiber Communication Conference and Exposition and the National Fiber Optic Engineers Conference* (2011), pp. 1–3.
8. B. G. Lee and N. Dupuis, J. Lightwave Technol. **37**, 6 (2019).
9. A. H. Atabaki, A. A. Eftekhar, S. Yegnanarayanan, and A. Adibi, Opt. Express **21**, 15706 (2013).
10. F. Gan, T. Barwicz, M. Popovic, M. Dahlem, C. Holzwarth, P. Rakich, H. Smith, E. Ippen, and F. Kartner, *Photonics in Switching* (2007), paper TuB3.3.
11. A. Masood, M. Pantouvaki, G. Lepage, P. Verheyen, J. V. Campenhout, P. Absil, D. V. Thourhout, and W. Bogaerts, *10th International Conference on Group IV Photonics* (2013), pp. 83–84.
12. D. T. Neilson, C. R. Doerr, D. M. Marom, R. Ryf, and M. P. Earnshaw, Bell Labs Tech. J. **11**, 105 (2006).
13. P. Dong, R. Shafiiha, S. Liao, H. Liang, N.-N. Feng, D. Feng, G. Li, X. Zheng, A. V. Krishnamoorthy, and M. Asghari, Opt. Express **18**, 10941 (2010).
14. Y. Shi, D. Dai, and S. He, Opt. Commun. **253**, 276 (2005).
15. J. D. Doménech, J. S. Fandiño, B. Gargallo, and P. Muñoz, J. Lightwave Technol. **32**, 2536 (2014).
16. Á. Rosa, A. Gutiérrez, A. Brimont, A. Griol, and P. Sanchis, Opt. Express **24**, 191 (2016).
17. D. Schall, M. Mohsin, A. A. Sagade, M. Otto, B. Chmielak, S. Suckow, A. L. Giesecke, D. Neumaier, and H. Kurz, Opt. Express **24**, 7871 (2016).
18. L. Yu, Y. Yin, Y. Shi, D. Dai, and S. He, Optica **3**, 159 (2016).
19. Y. Shi, Y. Ji, F. Hui, H. Wu, and M. Lanza, Nano Res. **7**, 1820 (2014).
20. P. Sun and R. M. Reano, Opt. Express **18**, 8406 (2010).
21. Z. Lu, K. Murray, H. Jayatilleka, and L. Chrostowski, *IEEE Photonics Conference (IPC)* (2016), pp. 107–110.
22. Y. Hashizume and K. Watanabe, *6th IEEE International Conference on Group IV Photonics* (2009), pp. 238–240.
23. Q. Fang, J. F. Song, T. Y. Liow, H. Cai, M. B. Yu, G. Q. Lo, and D. L. Kwong, IEEE Photon. Technol. Lett. **23**, 525 (2011).
24. M. R. Watts, J. Sun, C. DeRose, D. C. Trotter, R. W. Young, and G. N. Nielson, Opt. Lett. **38**, 733 (2013).
25. M. Jacques, A. Samani, E. El-Fiky, D. Patel, Z. Xing, and D. V. Plant, Opt. Express **27**, 10456 (2019).
26. K. Chen, F. Duan, and Y. Yu, Opt. Lett. **44**, 951 (2019).
27. F. Duan, K. Chen, S. Wang, L. Wei, Y. Yu, and D. Ban, Appl. Phys. Lett. **116**, 011102 (2020).
28. R. Halir, I. Molina-Fernandez, A. Ortega-Monux, J. G. Wanguemert-Perez, D. Xu, P. Cheben, and S. Janz, J. Lightwave Technol. **26**, 2928 (2008).
29. F. Duan, K. Chen, and Y. Yu, Opt. Commun. **439**, 239 (2019).
30. H. D. Espinosa and B. Prorok, J. Mater. Sci. **38**, 4125 (2003).
31. P. Dong, W. Qian, H. Liang, R. Shafiiha, D. Feng, G. Li, J. E. Cunningham, A. V. Krishnamoorthy, and M. Asghari, Opt. Express **18**, 20298 (2010).